ACS APPLIED POLYMER MATERIALS

pubs.acs.org/acsapm Article

Self-Assembly of Charged Diblock Copolymers with Reduced Backbone Polarity

Bo Zhang, Caini Zheng, Frank S. Bates,* and Timothy P. Lodge*

Cite This: ACS Appl. Polym. Mater. 2023, 5, 2223−2229 Read Online

ACCESS | Metrics & More | Article Recommendations | Supporting Information

ABSTRACT: Charged block copolymers that can self-assemble into a host of nanostructures offer a great opportunity as next-generation battery electrolytes with outstanding ionic conductivity and mechanical robustness. The impact of ions on the self-assembly of charged block copolymers, however, remains to be fully understood. In this article, we report the phase behavior of charged-neutral block copolymers where a relatively nonpolar matrix was employed in the charged block to boost the strength of electrostatic interaction. The phase behavior was established using small-angle X-ray scattering (SAXS). We found that the overall shape of the phase boundary between ordered and disordered states is asymmetric, tilting toward the charged block-lean side of the phase portrait. However, the composition windows of the ordered phases, such as lamellae and hexagonally packed cylinders observed in this study, are comparable to those of neutral diblock copolymers and are not obviously affected by the incorporation of charges. The results obtained in this work provide insight into the impact of ions on the self-assembly of charged block copolymers as well as the design of nanostructured polymer electrolytes.

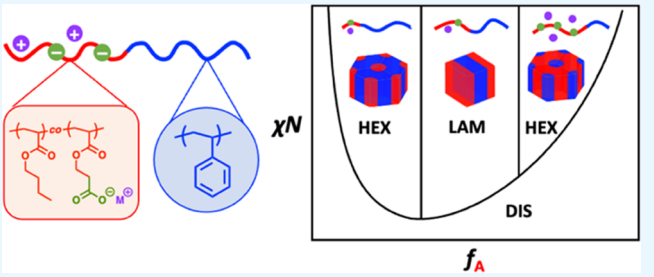

KEYWORDS: *charged block copolymers, ionomers, single-ion conductors, polymer electrolytes, self-assembly, phase behavior, X-ray scattering*

INTRODUCTION

Polymer electrolytes are of interest due to their outstanding thermal and chemical stability relative to conventional liquid electrolytes. Polymer electrolytes typically comprise poly(ethylene oxide) doped with a lithium salt, with ionic conductivity as high as 10^{-3} S/cm.[1] However, there are two significant limitations to this class of polymer electrolytes. First, mechanical robustness, desired to suppress lithium dendrite growth, is relatively poor due to low glass-transition temperatures. One solution for this problem is to design microphase-separated block copolymers (BCPs) that feature an ionic conductive domain as well as a mechanically robust domain.[2−18] The second limitation is the poor transference number of the lithium ion (*i.e.*, the ratio of the electric current carried by the lithium cation to the total current), which leads to electrode polarization and compromises battery performance.[2] This challenge can be overcome by covalently attaching anions to the polymer backbone, which substantially limits anion transport and leads to single-ion conducting polymer electrolytes.[19,20] Combining both solutions leads to the strategy of designing intrinsically charged BCPs that can microphase-separate into well-defined domains to provide outstanding ionic conductivity and mechanical stability simultaneously. However, the self-assembly of charged BCPs, which would provide indispensable insight into the rational design of polymer electrolytes, remains to be fully elucidated.

The phase behavior of neutral diblock copolymers is largely controlled by three parameters: block volume fraction f, degree of polymerization N, and Flory−Huggins interaction parameter χ.[21−23] Symmetric diblock copolymers ($f \approx 1/2$) form lamellae (LAM) at high segregation strength ($\chi N \gg 10$) and are disordered (DIS) at χN <10.5, where the order−disorder transition (ODT) occurs at $\chi N = 10.5$ within mean-field theory.[24] Increasing or decreasing block volume fraction leads to the formation of morphologies with nonzero curvatures, such as double gyroid (GYR), hexagonally packed cylinders (HEX), and body-centered cubic spheres (BCC).

Incorporation of charge has been shown by numerous experimental and theoretical investigations to produce significant and complex effects on the self-assembly of diblock copolymers. In salt-containing diblock copolymers, a commonly observed phenomenon is a linear increase in the effective interaction parameter (χ_{eff}) with increasing salt loading,[3,5−9,13,17,25−28] although more complex changes have also been observed.[7,29−32] Loo and Balsara organized

Received: December 23, 2022
Accepted: February 7, 2023
Published: February 16, 2023

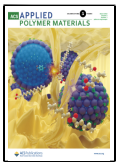

Scheme 1. Synthesis of the Charged Diblock Copolymers Used in This Study

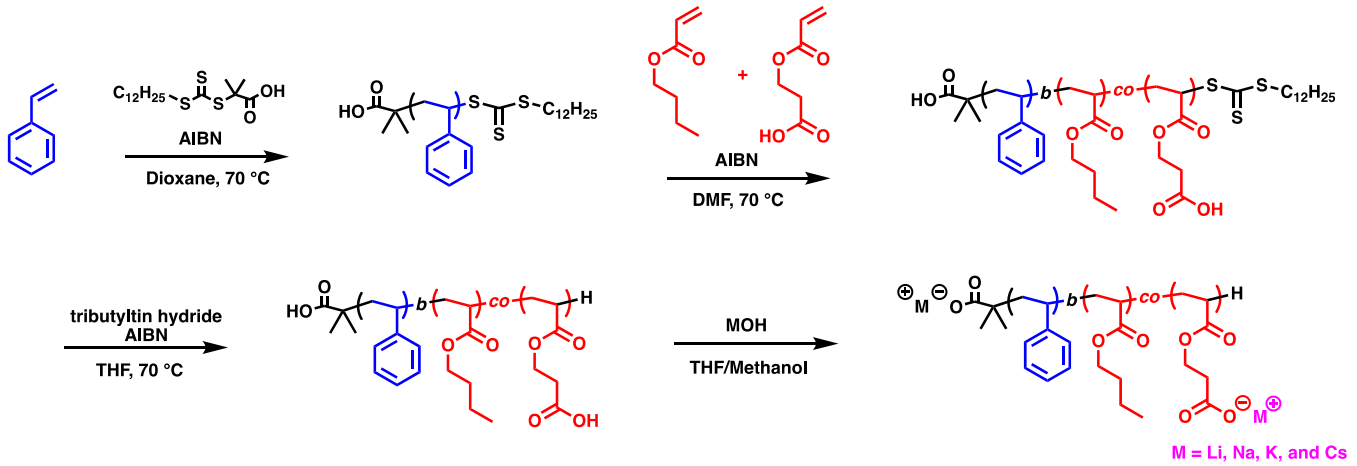

thermodynamic data obtained from polystyrene-*block*-poly(ethylene oxide) (PS-PEO) doped with lithium bis(trifluoromethanesulfonyl)imide (LiTFSI), using a linear relation between χ_{eff} and salt concentration, and demonstrated that the phase portrait overall mimics that of neutral diblock copolymers.[8,9] The phase behavior of intrinsically charged diblock copolymers, where ions are covalently attached to the polymer backbone, is even more complicated. For example, Park and Balsara reported that symmetric poly(4-styrenesulfonic acid)-*block*-poly(methyl butylene) can self-assemble into a series of morphologies including LAM, GYR, perforated LAM, and HEX at different levels of sulfonation, while only LAM is expected for symmetric neutral diblock copolymers.[33] Several studies also illustrated the existence of inverse HEX, where the minority charged block forms the continuous domain.[34−37] Unlike such unusual phase behavior, conventional phase behavior similar to that of neutral diblock copolymers has also been widely reported.[38−41] It was hypothesized that the strength of the electrostatic interaction is a key factor in determining whether conventional or unconventional phase behavior will be obtained.[36]

Several theories have been developed to elucidate the self-assembly of charged diblock copolymers.[34,35,42−59] For example, de la Cruz and co-workers developed a hybrid self-consistent field theory (SCFT) model that captures both local charge ordering and long-range polymer conformations simultaneously.[50−54] Applying this method to charged diblock copolymers, they demonstrated that the enhanced microphase separation caused by the counterion solvation effect can be quantitatively captured by a linear increase in the effective interaction parameter with increasing charge fraction, consistent with the results from Wang and co-workers who incorporated the Born solvation energy into SCFT calculations.[44−46,48,49] Besides counterion solvation, they also demonstrated that local ion clusters formed under strong electrostatic interaction can lead to phase portraits that tilt significantly toward low f_A, where f_A is the charged block volume fraction. Due to such asymmetric, "chimney"-like phase diagrams, unconventional morphologies including the inverse HEX mentioned before can be accessed by tuning the strength of electrostatic interaction or simply charge fraction.[50] There are other theories and simulations that show different predictions. For example, Qin and co-workers demonstrated that ion solvation energy alone can lead to skewed phase diagrams.[57,58] On the other hand, Gavrilov and co-workers demonstrated that microphase separation can be induced by electrostatic correlation alone. The predicted phase diagram only shows very subtle differences with the neutral counterpart.[60]

Recently, we studied the phase behavior of *symmetric* poly[(oligo(ethylene glycol) methyl ether methacrylate−*co*−oligo(ethylene glycol) propyl sodium sulfonate methacrylate)]-*block*-polystyrene (PsOEGMA-PS) diblock copolymers as a function of charge fraction and molecular weight.[61] We found that the ordered morphology remains LAM with increasing charge fraction, while χ_{eff} increases linearly with respect to charge fraction. This phenomenon indicates the dominance of the counterion solvation effect, which was attributed to the significant difference between the dielectric constants of the two blocks. In this work, we describe the phase behavior of a different model system where the matrix of the charged block is replaced with poly(butyl acrylate) such that the dielectric constant of the charged block is reduced compared to that in our previous study and should be much closer to that of the neutral polystyrene block. The relatively nonpolar charged block reduces the mismatch in the dielectric constant of each block but boosts the strength of the electrostatic interaction. The overall phase boundary between the ordered and disordered states was found to be asymmetric and skews toward the charged block-lean side of the phase portrait. However, the composition windows of the ordered phases are not obviously affected and closely resemble those of neutral diblock copolymers. This suggests that the predicted asymmetric phase diagrams with substantially impacted ordered phase locations are not readily obtained, especially because nonpolar blocks are rarely employed due to poor ionic conductivity. The higher dielectric constants associated with the more polar charged blocks greatly reduce the electrostatic interaction, leading to the dominance of the counterion solvation effect and therefore a linear increase in χ_{eff} with increasing charge fraction.

EXPERIMENTAL SECTION

Polymer Synthesis. The model system, poly(butyl acrylate-*co*-2-carboxyethyl acrylate)-*block*-polystyrene (SBA), was prepared using reversible addition-fragmentation chain transfer polymerization (RAFT) followed by post-modifications. A polystyrene macro chain transfer agent was first synthesized, which was extended with the acid-containing block and then converted to charged polymers with

https://doi.org/10.1021/acsapm.2c02220
ACS Appl. Polym. Mater. 2023, 5, 2223−2229

different metal cations. Scheme 1 presents the major synthetic steps of these materials, and the details are described in the Supporting Information.

Determination of Reactivity Ratios. Monomer reactivity ratios were determined to characterize the distribution of charged monomers along the polymer backbone. Six reactions with different feed ratios of CEA and BA monomers ranging from 0.1 to 0.9 were carried out under the same reaction conditions as described in the previous section. Initial feed ratios and monomer consumption were determined using proton nuclear magnetic resonance spectroscopy (^{1}H-NMR). Total monomer conversions were kept below 15% so that composition drift during the reaction can be neglected. Composition data were fit with eq 1 to determine the reactivity ratios r_{12} and r_{21}, where 1 and 2 represent CEA and BA, respectively.[62]

$$F_1 = \frac{r_{12}f_1^2 + f_1f_2}{r_{12}f_1^2 + 2f_1f_2 + r_{21}f_2^2} \quad (1)$$

Proton Nuclear Magnetic Resonance (^{1}H-NMR) Spectroscopy. ^{1}H-NMR spectra were collected using a Bruker Avance III HD Nanobay AX-400 spectrometer. Deuterated chloroform ($CDCl_3$) was used as the solvent. Selected NMR spectra for samples with different charge fractions and volume fractions of the charged block copolymers are presented in Figures S1 and S2.

Size Exclusion Chromatography (SEC). Molecular weights and dispersities were determined via size exclusion chromatography (SEC) using tetrahydrofuran (THF) as the eluent; ^{1}H NMR was also employed to determine the number-average molecular weight. The SEC instrument is equipped with a Wyatt OptiLab EX refractive index detector and a Wyatt DAWN DSP light scattering detector. SEC traces from all of the specimens are presented in Figure S3.

Differential Scanning Calorimetry (DSC). DSC experiments were performed to measure the glass-transition temperatures of the charged diblock copolymers. Samples were hermetically sealed in Tzero DSC pans under air and measured with a DSC Q1000 from TA Instruments. Each pan was loaded at 40 °C, heated to 110 °C at 10 °C/min, held for 1 min, cooled to −100 °C at 10 °C/min, held for 5 min, and heated to 130 °C at 10 °C/min.

Small-Angle X-ray Scattering (SAXS). SAXS measurements were performed on a Xenocs GANESHA instrument, which is equipped with an Eiger 1M (Dectris) detector. Samples for SAXS measurements were loaded between two Teflon washers and a Viton O-ring, sandwiched between two Kapton films, and sealed in stainless-steel cells. The stainless-steel cells were then loaded into a customized INSTEC heating stage where the temperature was controlled by an INSTEC MK2000 precision temperature controller. Samples were annealed at 110 °C for only 10 min before measurements to avoid potential sample degradation. Selected samples were measured after a longer annealing time, and no apparent difference was observed, indicating that the samples had likely been annealed sufficiently after 10 min. Isotropic two-dimensional (2D) scattering patterns were reduced to the one-dimensional (1D) form of scattering intensity *versus* the magnitude of the scattering wavevector $q = 4\pi \sin(\theta/2)/\lambda$ using the SAXSGUI software, where θ is the scattering angle and λ = 1.54 Å is the wavelength. The q scale was calibrated using silver behenate.

RESULTS AND DISCUSSION

Table 1 summarizes the molecular weight, dispersity, volume fraction, and charge fraction of each specimen reported in this work. In this study, two sets of polymers with 15 and 30% charge fractions were prepared. Each acid-containing precursor polymer was converted to charged polymers with a series of metal cations, including Li^+, Na^+, K^+, and Cs^+. Within each set of samples, the volume fraction of the charged block was changed to cover the entire phase diagram. Reactivity ratios of BA and CEA were determined to characterize the charge distribution along the backbone in the final products. Figure 1

Table 1. Summary of Polymer Characteristics

name[a]	x[b]	f_{PBA}[c]	M_n (kg/mol)	$Đ$
$SBA_{0.15}(24,18)$	0.15	0.18	24	1.11
$SBA_{0.15}(28,30)$	0.15	0.30	28	1.19
$SBA_{0.15}(33,40)$	0.15	0.40	33	1.07
$SBA_{0.15}(22,44)$	0.15	0.44	22	1.09
$SBA_{0.15}(24,49)$	0.15	0.49	24	1.12
$SBA_{0.15}(23,63)$	0.15	0.63	23	1.12
$SBA_{0.15}(39,68)$	0.15	0.68	39	1.14
$SBA_{0.29}(25,23)$	0.29	0.23	25	1.10
$SBA_{0.30}(24,48)$	0.30	0.48	24	1.11
$SBA_{0.30}(27,68)$	0.30	0.68	27	1.10
$SBA_{0.30}(42,70)$	0.30	0.70	42	1.17

[a]$SBA_x(m,n)$ is used to name the polymers, where x is the mole fraction of charged monomers in the BA block, m is the number-average molecular weight in kDa determined using SEC, and n is the charged block volume fraction in %. [b]Mole fractions (x) of charged monomers determined using ^{1}H-NMR spectroscopy. [c]Volume fraction of the BA block with H^+, obtained using the melt density of PS = 1.05 g/cm^3 and melt densities of BA_0 = 1.08 g/cm^3 and $BA_{1.00}$ = 1.36 g/cm^3, which were estimated using a group contribution method.[63] Changing cations may vary the volume fraction by at most 4%, assuming the density remains unchanged.

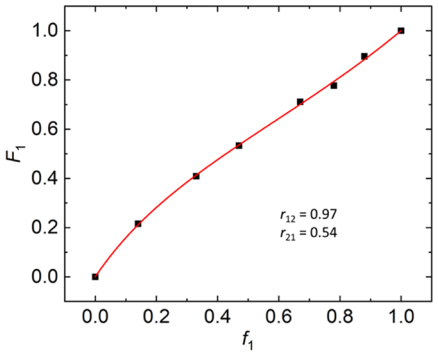

Figure 1. Determination of reactivity ratios by fitting the composition data of the polymer composition versus monomer feed composition with eq 1. The black squares are experimental results, the red line is the fitted curve, and 1 and 2 are CEA and BA, respectively.

presents a plot of polymer composition versus feed ratio along with the fit to eq 1, leading to r_{12} = 0.96 and r_{21} = 0.54. These values suggest a modest enrichment of CEA monomers at low monomer conversions. However, we do not anticipate a significant effect on the phase behavior caused by this small composition gradient.

DSC measurements were carried out to study the thermal transitions of these materials. Figure 2 demonstrates the glass-transition temperatures of the volumetrically symmetric samples with 15 and 30% charge fractions. Replacing Li^+ with larger metal cations gradually decreases T_g, as shown in Figure 2a. Figure 2b shows a similar trend, and the higher charge content leads to higher T_g for each case. This is consistent with previous results where increasing the charge fraction/ion content leads to stronger ion−dipole interaction, which in turn raises T_g.[64,65] It should be noted that Cs^+-containing samples show similar T_g's despite the different charge fractions. The origin of this phenomenon is not clear and further experiments may be warranted. The glass-transition temperature of polystyrene, approximately 90 °C, is therefore significantly higher than the ionomer block. We studied the

https://doi.org/10.1021/acsapm.2c02220
ACS Appl. Polym. Mater. 2023, 5, 2223−2229

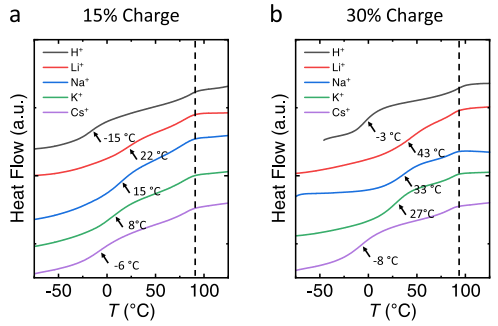

Figure 2. DSC results for volumetrically symmetric polymers with (a) 15% charge fraction and (b) 30% charge fraction. Vertical dashed lines refer to the T_g of the polystyrene block.

phase behavior of the model system at 110 °C, which should provide sufficient polymer segmental motions while preventing polymer degradation.

Figures 3 and 4 present two series of SAXS patterns for SBA with 15 and 30% charge fractions, respectively, obtained at 110 °C. Within each series, the volume fraction of the charged block f_{BA} ranges from 0.18 to 0.68 for 15% charge fraction and from 0.23 to 0.70 for 30% charge fraction, covering most of the phase portrait for each case. Each subfigure presents the scattering patterns from a single precursor polymer but with different counterions (H^+, Li^+, Na^+, K^+, and Cs^+).

Figure 3 shows four samples with similar molecular weights, enabling comparison of morphologies at essentially the same segregation strength among samples with the same counterion. In fact, counterion identity impacts χ_{eff} substantially, as is evident in Figure 3b,c. Both acid versions (H^+) show ordered morphologies that transition to disordered when Li^+ is substituted for H^+, indicating a decrease in χ_{eff}. The stronger segregation strength associated with the acid version is likely due to hydrogen bonding among carboxylic acid groups. Replacing Li^+ with larger ions Na^+, K^+, and Cs^+ increases χ_{eff}, as evidenced by the appearance of ordered morphologies indicated by a sharp scattering peak in the case of Cs^+ in Figure 3b and Na^+ in Figure 3c. It should be noted that $SBA_{0.15}(24,49)$ with Na^+ shown in Figure 3c is likely in a state of ordered/disordered coexistence. Similar behavior is also shown in Figure 3d, where the samples with H^+, K^+, and Cs^+ appear to be disordered according to the single broad scattering peak, while those with Li^+ and Na^+ are almost homogeneous based on the reduced peak intensities. This trend is contradictory to the previous results from salt-doped diblock copolymers,[3] where larger ions lead to lower χ_{eff} due to the smaller difference in the Born solvation energy between the ion dissolving in each block.[45,46] One possible cause for the increase in χ_{eff} is the reduced electrostatic cohesion effect due to larger cations.[50] Microphase separation is suppressed across the majority of the phase portrait but enhanced at low volume fractions of the charged block, when electrostatic cohesion is strong, according to Sing et al.[50] Larger ions decrease the strength of the electrostatic interaction, therefore reducing the extent of microphase separation suppression and increasing χ_{eff}.

We also estimated the shape of the phase boundary between ordered and disordered states from the results presented in Figure 3. Figure 3c demonstrates that symmetric $SBA_{0.15}(24,49)$ forms ordered structures, except with Li^+ as the counterion, which is disordered, and likely ordered/disordered coexistence with Na^+. The sample with a slightly lower molecular weight and volume fraction, $SBA_{0.15}(22,44)$, is disordered when the counterions are Li^+, Na^+, and K^+, but adopts an ordered morphology with H^+ and Cs^+. Changing the volume fraction to 0.18 and 0.63 leads to disorder across all samples. This suggests that $(\chi N)_{ODT}$ for symmetric diblock copolymers is lower than that of asymmetric analogs, similar to neutral block copolymers. Additionally, the scattering peaks from $SBA_{0.15}(24,63)$ (Figure 3d) are much lower in intensity than those from $SBA_{0.15}(24,18)$ as shown in Figure 3a, indicating that the phase boundary at low f_{BA} appears at lower χN than that at high f_{BA}, to some extent similar to the chimney-like phase portrait predicted by theoretical studies.[50,57] Such an asymmetric ODT boundary is also observed at a higher charge fraction, as discussed below. Although we were able to estimate the overall shape of the phase boundary, we could not identify the exact ordered morphologies formed at this molecular weight due to the lack of higher-order reflection peaks. Absence of higher-order peaks is attributable to the close proximity to the ODTs for these samples. To tackle this challenge, the molecular weight was increased to boost the overall segregation strength. Figure S4 illustrates the results from three polymers with the same 15% charge fraction but with higher molecular weights. Unfortunately, only $SBA_{0.15}(33,40)$ exhibits higher-order diffraction peaks that can be indexed to LAM ($q/q^* = 1, 2, 3$), therefore preventing us from obtaining an actual phase portrait.

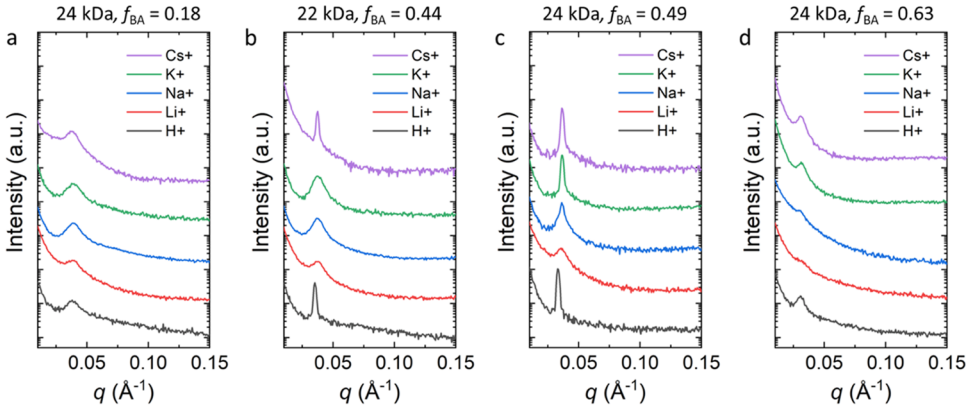

Figure 3. SAXS patterns for charged diblock copolymers (a) $SBA_{0.15}(24,18)$, (b) $SBA_{0.15}(22,44)$, (c) $SBA_{0.15}(24,49)$, and (d) $SBA_{0.15}(24,63)$. Each figure contains the results from a given polymer but with different counterions.

https://doi.org/10.1021/acsapm.2c02220
ACS Appl. Polym. Mater. 2023, 5, 2223−2229

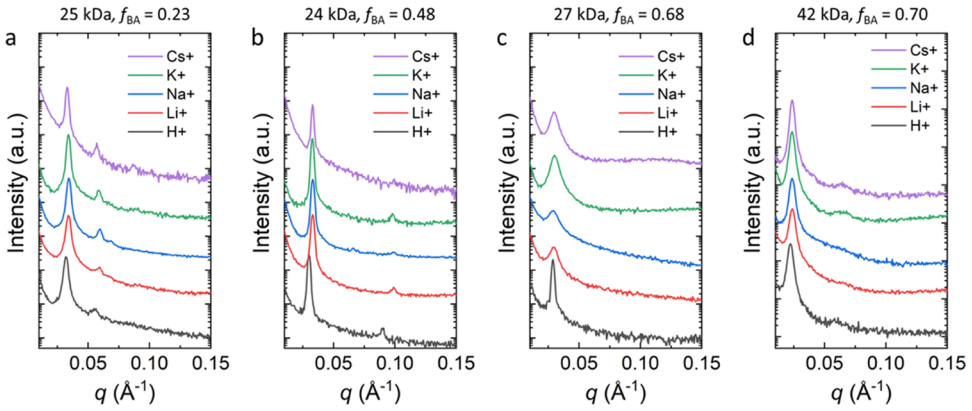

Figure 4. SAXS patterns for charged diblock copolymers (a) $SBA_{0.3}$(25,23), (b) $SBA_{0.3}$(24,48), (c) $SBA_{0.3}$(27,68), and (d) $SBA_{0.3}$(42,70). Each figure contains the results from a single polymer but with different counterions.

The phase behavior of the same model system but with a higher charge fraction was also investigated. Figure 4 presents the SAXS results from samples with 30% charge fraction but different volume fractions that range from 0.23 to 0.70. The scattering patterns from $SBA_{0.3}$(25,23), presented in Figure 4a, can be indexed with $q/q^* = 1, \sqrt{3}, \sqrt{4}$, consistent with HEX. Additionally, there is little variation among the samples with different counterions. Figure 4b presents the results from $SBA_{0.3}$(24,48), and the scattering patterns can be indexed with $q/q^* = 1, 2, 3$, consistent with LAM. The missing peak at $q/q^* = 2$ is likely due to form factor extinction produced by symmetric lamellae. It is more challenging to evaluate the phase behavior of samples on the other side of the phase portrait, again due to the lack of higher-order scattering peaks. $SBA_{0.3}$(27,68) exhibits DIS for all cases with metal cations, while the acid version forms an ordered morphology, which again can be attributed to the hydrogen bond among carboxylic acid groups. Since the samples presented in Figure 4a–c have similar molecular weights, we conclude that $(\chi N)_{ODT}$ is much lower for samples rich in the charged block than that of samples lean in the charged block. This observation corroborates the conclusion from the prior case of 15% charge fraction that an asymmetric, chimney-like ODT boundary is obtained. It is not clear, however, whether $(\chi N)_{ODT}$ at low f_{BA} is higher or lower than that at f_{BA} = 0.5 from the current results. To identify the ordered morphology at $f_{BA} > 0.5$, we synthesized another polymer with a much higher-molecular-weight $SBA_{0.3}$(42,70), and the results are shown in Figure 4d. Unfortunately, there are still no clear higher-order peaks, except for a small peak at $q/q^* = \sqrt{3}$ for the specimen with Cs^+ and a broad feature at higher q for all of the scattering patterns. Due to the peak at $q/q^* = \sqrt{3}$ and the hump at higher q that is consistent with the cylinder form factor profile as shown in Figure S5, we suspect this sample is associated with HEX. If this is true, then the overall composition windows of LAM and HEX on both sides remain largely unchanged from those of neutral diblock copolymers. We present a highly simplified sketch of the proposed phase diagram, as shown in Figure 5, to help demonstrate the asymmetric ODT boundary but unchanged ordered phase locations. Interestingly, the phase diagram that we proposed here is similar to the results obtained in a recent simulation study, where the microphase separation is induced solely by electrostatic correlation.[60]

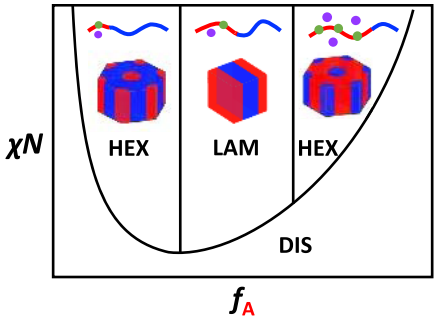

Figure 5. Schematic illustration of charged diblock copolymers with a relatively nonpolar charged block, based on the results obtained in this model system. It should be noted that the cartoon is highly simplified and may not accurately describe the phase behavior due to the limited number of samples.

Several investigations on charged BCPs have demonstrated skewed phase diagrams including substantially shifted ordered phase locations, such as the formation of inverse HEX phase, where the minority charged block forms the matrix.[35−37] In these studies, however, other factors besides electrostatic interaction that can lead to the formation of this morphology have been identified. One example is the extreme conformational asymmetry due to bulky ionic moieties,[36,37] which alone can significantly skew the phase diagram.[66] It is therefore difficult to determine whether electrostatic cohesion is the dominant factor. In fact, in our model system, conformational asymmetry is minimal compared to those studies, and we were not able to find any evidence of inverse HEX. Together, these results suggest that highly tilted phase portraits with significantly shifted locations of ordered phases are difficult to achieve. In practice, polar blocks with high dielectric constants are most often employed to maximize ionic conductivity. Under these conditions, electrostatic interaction is likely relatively weak. Due to the large mismatch in the dielectric constant of each block, the dominant impact from the incorporation of charges is likely the counterion solvation effect, which increases the effective interaction parameter χ_{eff} linearly with increasing charge fraction.

CONCLUSIONS

In summary, we investigated the phase behavior of polystyrene-*block*-poly(butyl acrylate-*co*-carboxyethyl acrylate) with various metal cations. We found that the ODT boundary

https://doi.org/10.1021/acsapm.2c02220
ACS Appl. Polym. Mater. 2023, 5, 2223−2229

of the phase portrait is slightly asymmetric, tilting toward the charged block-lean side and to some extent mimicking the predicted chimney-like phase portrait. However, the composition windows of the ordered phases are not obviously affected by the incorporation of charges. These results indicate that highly skewed phase diagrams with shifted ordered phase locations are not so easy to obtain, even with a relatively nonpolar charged block. Overall, the results obtained in this work provide valuable insight into the phase behavior of charged block copolymers and ultimately the design of nanostructured polymer electrolytes.

■ ASSOCIATED CONTENT

Supporting Information

The Supporting Information is available free of charge at https://pubs.acs.org/doi/10.1021/acsapm.2c02220.

Synthetic procedures, SEC traces, NMR spectra, and SAXS patterns (PDF)

■ AUTHOR INFORMATION

Corresponding Authors

Frank S. Bates − *Department of Chemical Engineering and Materials Science, University of Minnesota, Minneapolis, Minnesota 55455, United States;* orcid.org/0000-0003-3977-1278; Email: bates001@umn.edu

Timothy P. Lodge − *Department of Chemical Engineering and Materials Science and Department of Chemistry, University of Minnesota, Minneapolis, Minnesota 55455, United States;* orcid.org/0000-0001-5916-8834; Email: lodge@umn.edu

Authors

Bo Zhang − *Department of Chemical Engineering and Materials Science, University of Minnesota, Minneapolis, Minnesota 55455, United States;* orcid.org/0000-0001-5366-1855

Caini Zheng − *Department of Chemistry, University of Minnesota, Minneapolis, Minnesota 55455, United States*

Complete contact information is available at: https://pubs.acs.org/10.1021/acsapm.2c02220

Notes

The authors declare no competing financial interest.

■ ACKNOWLEDGMENTS

This work was supported by the Office of Basic Energy Sciences (BES) of the U.S. Department of Energy (DoE), under Contract No. DE-SC0017809. Parts of this work were carried out in the Characterization Facility at the University of Minnesota, which receives partial support from the NSF through the MRSEC program (DMR-2011401).

■ REFERENCES

(1) Xue, Z.; He, D.; Xie, X. Poly(ethylene oxide)-based electrolytes for lithium-ion batteries. *J. Mater. Chem. A* **2015**, *3*, 19218−19253.

(2) Hallinan, D. T.; Balsara, N. P. Polymer Electrolytes. *Annu. Rev. Mater. Res.* **2013**, *43*, 503−525.

(3) Young, W. S.; Epps, T. H. Salt doping in PEO-containing block copolymers: Counterion and concentration effects. *Macromolecules* **2009**, *42*, 2672−2678.

(4) Chintapalli, M.; Le, T. N. P.; Venkatesan, N. R.; Mackay, N. G.; Rojas, A. A.; Thelen, J. L.; Chen, X. C.; Devaux, D.; Balsara, N. P. Structure and Ionic Conductivity of Polystyrene-block-poly(ethylene oxide) Electrolytes in the High Salt Concentration Limit. *Macromolecules* **2016**, *49*, 1770−1780.

(5) Wanakule, N. S.; Panday, A.; Mullin, S. A.; Gann, E.; Hexemer, A.; Balsara, N. P. Ionic conductivity of block copolymer electrolytes in the vicinity of order-disorder and order-order transitions. *Macromolecules* **2009**, *42*, 5642−5651.

(6) Wanakule, N. S.; Virgili, J. M.; Teran, A. A.; Wang, Z. G.; Balsara, N. P. Thermodynamic Properties of Block Copolymer Electrolytes Containing Imidazolium and Lithium Salts. *Macromolecules* **2010**, *43*, 8282−8289.

(7) Teran, A. A.; Balsara, N. P. Thermodynamics of block copolymers with and without salt. *J. Phys. Chem. B* **2014**, *118*, 4−17.

(8) Loo, W. S.; Balsara, N. P. Organizing thermodynamic data obtained from multicomponent polymer electrolytes: Salt-containing polymer blends and block copolymers. *J. Polym. Sci., Part B: Polym. Phys.* **2019**, *57*, 1177−1187.

(9) Loo, W. S.; Galluzzo, M. D.; Li, X.; Maslyn, J. A.; Oh, H. J.; Mongcopa, K. I.; Zhu, C.; Wang, A. A.; Wang, X.; Garetz, B. A.; Balsara, N. P. Phase Behavior of Mixtures of Block Copolymers and a Lithium Salt. *J. Phys. Chem. B* **2018**, *122*, 8065−8074.

(10) Ioannou, E. F.; Mountrichas, G.; Pispas, S.; Kamitsos, E. I.; Floudas, G. Lithium ion induced nanophase ordering and ion mobility in ionic block copolymers. *Macromolecules* **2008**, *41*, 6183−6190.

(11) Gartner, T. E.; Morris, M. A.; Shelton, C. K.; Dura, J. A.; Epps, T. H. Quantifying lithium salt and polymer density distributions in nanostructured ion-conducting block polymers. *Macromolecules* **2018**, *51*, 1917−1926.

(12) Morris, M. A.; Sung, S. H.; Ketkar, P. M.; Dura, J. A.; Nieuwendaal, R. C.; Epps, T. H. Enhanced Conductivity via Homopolymer-Rich Pathways in Block Polymer-Blended Electrolytes. *Macromolecules* **2019**, *52*, 9682−9692.

(13) Epps, T. H.; Bailey, T. S.; Waletzko, R.; Bates, F. S. Phase behavior and block sequence effects in lithium perchlorate-doped poly(isoprene-b-styrene-b-ethylene oxide) and poly(styrene-b-isoprene-b-ethylene oxide) triblock copolymers. *Macromolecules* **2003**, *36*, 2873−2881.

(14) Xie, S.; Meyer, D. J.; Wang, E.; Bates, F. S.; Lodge, T. P. Structure and Properties of Bicontinuous Microemulsions from Salt-Doped Ternary Polymer Blends. *Macromolecules* **2019**, *52*, 9693−9702.

(15) Xie, S.; Zhang, B.; Bates, F. S.; Lodge, T. P. Phase Behavior of Salt-Doped A/B/AB Ternary Polymer Blends: The Role of Homopolymer Distribution. *Macromolecules* **2021**, *54*, 6990−7002.

(16) Zheng, C.; Zhang, B.; Bates, F. S.; Lodge, T. P. Self-Assembly of Partially Charged Diblock Copolymer-Homopolymer Ternary Blends. *Macromolecules* **2022**, *55*, 4766−4775.

(17) Naidu, S.; Ahn, H.; Gong, J.; Kim, B.; Ryu, D. Y. Phase Behavior and Ionic Conductivity of Lithium Perchlorate-Doped Polystyrene-b-poly(2-vinylpyridine) Copolymer. *Macromolecules* **2011**, *44*, 6085−6093.

(18) Singh, M.; Odusanya, O.; Wilmes, G. M.; Eitouni, H. B.; Gomez, E. D.; Patel, A. J.; Chen, V. L.; Park, M. J.; Fragouli, P.; Iatrou, H.; Hadjichristidis, N.; Cookson, D.; Balsara, N. P. Effect of molecular weight on the mechanical and electrical properties of block copolymer electrolytes. *Macromolecules* **2007**, *40*, 4578−4585.

(19) Zhang, H.; Li, C.; Piszcz, M.; Coya, E.; Rojo, T.; Rodriguez-Martinez, L. M.; Armand, M.; Zhou, Z. Single lithium-ion conducting solid polymer electrolytes: advances and perspectives. *Chem. Soc. Rev.* **2017**, *46*, 797−815.

(20) Zhu, J.; Zhang, Z.; Zhao, S.; Westover, A. S.; Belharouak, I.; Cao, P. F. Single-Ion Conducting Polymer Electrolytes for Solid-State Lithium-Metal Batteries: Design, Performance, and Challenges. *Adv. Energy Mater.* **2021**, *11*, No. 2002836.

(21) Flory, P. J. Thermodynamics of high polymer solutions. *J. Chem. Phys.* **1942**, *10*, 51−61.

(22) Huggins, M. L. Theory of solutions of high polymers. *J. Am. Chem. Soc.* **1942**, *64*, 1712−1719.

(23) Huggins, M. L. Solutions of Long Chain Compounds. *J. Chem. Phys.* **1941**, *9*, 440.

(24) Leibler, L. Theory of Microphase Separation in Block Copolymers. *Macromolecules* **1980**, *13*, 1602−1617.
(25) Ruzette, A. V. G.; Soo, P. P.; Sadoway, D. R.; Mayes, A. M. Melt-formable block copolymer electrolytes for lithium rechargeable batteries. *J. Electrochem. Soc.* **2001**, *148*, A537−A543.
(26) Wang, J. Y.; Chen, W.; Russell, T. P. Ion-complexation-induced changes in the interaction parameter and the chain conformation of PS-b-PMMA copolymers. *Macromolecules* **2008**, *41*, 4904−4907.
(27) Gunkel, I.; Thurn-Albrecht, T. Thermodynamic and structural changes in ion-containing symmetric diblock copolymers: A small-angle X-ray scattering study. *Macromolecules* **2012**, *45*, 283−291.
(28) Thelen, J. L.; Inceoglu, S.; Venkatesan, N. R.; Mackay, N. G.; Balsara, N. P. Relationship between Ion Dissociation, Melt Morphology, and Electrochemical Performance of Lithium and Magnesium Single-Ion Conducting Block Copolymers. *Macromolecules* **2016**, *49*, 9139−9147.
(29) Qin, J.; de Pablo, J. J. Ordering Transition in Salt-Doped Diblock Copolymers. *Macromolecules* **2016**, *49*, 3630−3638.
(30) Grzetic, D. J.; Delaney, K. T.; Fredrickson, G. H. Field-Theoretic Study of Salt-Induced Order and Disorder in a Polarizable Diblock Copolymer. *ACS Macro Lett.* **2019**, *8*, 962−967.
(31) Loo, W. S.; Sethi, G. K.; Teran, A. A.; Galluzzo, M. D.; Maslyn, J. A.; Oh, H. J.; Mongcopa, K. I.; Balsara, N. P. Composition Dependence of the Flory−Huggins Interaction Parameters of Block Copolymer Electrolytes and the Isotaksis Point. *Macromolecules* **2019**, *52*, 5590−5601.
(32) Loo, W. S.; Jiang, X.; Maslyn, J. A.; Oh, H. J.; Zhu, C.; Downing, K. H.; Balsara, N. P. Reentrant phase behavior and coexistence in asymmetric block copolymer electrolytes. *Soft Matter* **2018**, *14*, 2789−2795.
(33) Park, M. J.; Balsara, N. P. Phase behavior of symmetric sulfonated block copolymers. *Macromolecules* **2008**, *41*, 3678−3687.
(34) Goswami, M.; Kumar, R.; Sumpter, B. G.; Mays, J. Breakdown of inverse morphologies in charged diblock copolymers. *J. Phys. Chem. B* **2011**, *115*, 3330−3338.
(35) Goswami, M.; Sumpter, B. G.; Huang, T.; Messman, J. M.; Gido, S. P.; Isaacs-Sodeye, A. I.; Mays, J. W. Tunable morphologies from charged block copolymers. *Soft Matter* **2010**, *6*, 6146.
(36) Russell, S. T.; Raghunathan, R.; Jimenez, A. M.; Zhang, K.; Brucks, S. D.; Iacob, C.; West, A. C.; Gang, O.; Campos, L. M.; Kumar, S. K. Impact of Electrostatic Interactions on the Self-Assembly of Charge-Neutral Block Copolyelectrolytes. *Macromolecules* **2020**, *53*, 548−557.
(37) Zhang, W.; Liu, Y.; Jackson, A. C.; Savage, A. M.; Ertem, S. P.; Tsai, T. H.; Seifert, S.; Beyer, F. L.; Liberatore, M. W.; Herring, A. M.; Coughlin, E. B. Achieving Continuous Anion Transport Domains Using Block Copolymers Containing Phosphonium Cations. *Macromolecules* **2016**, *49*, 4714−4722.
(38) Scalfani, V. F.; Wiesenauer, E. F.; Ekblad, J. R.; Edwards, J. P.; Gin, D. L.; Bailey, T. S. Morphological Phase Behavior of Poly(RTIL)-Containing Diblock Copolymer Melts. *Macromolecules* **2012**, *45*, 4262−4276.
(39) Weber, R. L.; Ye, Y.; Schmitt, A. L.; Banik, S. M.; Elabd, Y. A.; Mahanthappa, M. K. Effect of nanoscale morphology on the conductivity of polymerized ionic liquid block copolymers. *Macromolecules* **2011**, *44*, 5727−5735.
(40) Choi, J. H.; Ye, Y.; Elabd, Y. A.; Winey, K. I. Network Structure and Strong Microphase Separation for High Ion Conductivity in Polymerized Ionic Liquid Block Copolymers. *Macromolecules* **2013**, *46*, 5290−5300.
(41) Cotanda, P.; Sudre, G.; Modestino, M. A.; Chen, X. C.; Balsara, N. P. High anion conductivity and low water uptake of phosphonium containing diblock copolymer membranes. *Macromolecules* **2014**, *47*, 7540−7547.
(42) Marko, J. F.; Rabin, Y. Microphase Separation of Charged Diblock Copolymers: Melts and Solutions. *Macromolecules* **1992**, *25*, 1503−1509.
(43) Kumar, R.; Muthukumar, M. Microphase separation in polyelectrolytic diblock copolymer melt: Weak segregation limit. *J. Chem. Phys.* **2007**, *126*, No. 214902.
(44) Wang, Z. G. Effects of ion solvation on the miscibility of binary polymer blends. *J. Phys. Chem. B* **2008**, *112*, 16205−16213.
(45) Nakamura, I.; Balsara, N. P.; Wang, Z. G. Thermodynamics of Ion-Containing Polymer Blends and Block Copolymers. *Phys. Rev. Lett.* **2011**, *107*, No. 198301.
(46) Nakamura, I.; Wang, Z. G. Salt-doped block copolymers: ion distribution, domain spacing and effective chi parameter. *Soft Matter* **2012**, *8*, 9356−9367.
(47) Wang, X.; Goswami, M.; Kumar, R.; G Sumpter, B.; Mays, J. Morphologies of block copolymers composed of charged and neutral blocks. *Soft Matter* **2012**, *8*, 3036.
(48) Nakamura, I.; Balsara, N. P.; Wang, Z. G. First-Order Disordered-to-Lamellar Phase Transition in Lithium Salt-Doped Block Copolymers. *ACS Macro Lett.* **2013**, *2*, 478−481.
(49) Nakamura, I.; Wang, Z. G. Thermodynamics of Salt-Doped Block Copolymers. *ACS Macro Lett.* **2014**, *3*, 708−711.
(50) Sing, C. E.; Zwanikken, J. W.; Olvera De La Cruz, M. Electrostatic control of block copolymer morphology. *Nat. Mater.* **2014**, *13*, 694−698.
(51) Sing, C. E.; Olvera De La Cruz, M. Polyelectrolyte blends and nontrivial behavior in effective flory-huggins parameters. *ACS Macro Lett.* **2014**, *3*, 698−702.
(52) Sing, C. E.; Zwanikken, J. W.; Olvera de la Cruz, M. Theory of melt polyelectrolyte blends and block copolymers: phase behavior, surface tension, and microphase periodicity. *J. Chem. Phys.* **2015**, *142*, No. 034902.
(53) Jiménez-Ángeles, F.; Kwon, H. K.; Sadman, K.; Wu, T.; Shull, K. R.; Olvera de la Cruz, M. Self-Assembly of Charge-Containing Copolymers at the Liquid-Liquid Interface. *ACS Cent. Sci.* **2019**, *5*, 688−699.
(54) Pryamitsyn, V. A.; Kwon, H. K.; Zwanikken, J. W.; Olvera De La Cruz, M. Anomalous Phase Behavior of Ionic Polymer Blends and Ionic Copolymers. *Macromolecules* **2017**, *50*, 5194−5207.
(55) Yang, S.; Vishnyakov, A.; Neimark, A. V. Self-assembly in block polyelectrolytes. *J. Chem. Phys.* **2011**, *134*, No. 054104.
(56) Shen, K. H.; Hall, L. M. Effects of Ion Size and Dielectric Constant on Ion Transport and Transference Number in Polymer Electrolytes. *Macromolecules* **2020**, *53*, 10086−10096.
(57) Hou, K. J.; Qin, J. Solvation and Entropic Regimes in Ion-Containing Block Copolymers. *Macromolecules* **2018**, *51*, 7463−7475.
(58) Hou, K. J.; Loo, W. S.; Balsara, N. P.; Qin, J. Comparing Experimental Phase Behavior of Ion-Doped Block Copolymers with Theoretical Predictions Based on Selective Ion Solvation. *Macromolecules* **2020**, *53*, 3956−3966.
(59) Brown, J. R.; Seo, Y.; Hall, L. M. Ion Correlation Effects in Salt-Doped Block Copolymers. *Phys. Rev. Lett.* **2018**, *120*, No. 127801.
(60) Gavrilov, A. A.; Chertovich, A. V.; Potemkin, I. I. Phase Behavior of Melts of Diblock-Copolymers with One Charged Block. *Polymers* **2019**, *11*, 1027.
(61) Zhang, B.; Zheng, C.; Sims, M. B.; Bates, F. S.; Lodge, T. P. Influence of Charge Fraction on the Phase Behavior of Symmetric Single-Ion Conducting Diblock Copolymers. *ACS Macro Lett.* **2021**, *10*, 1035−1040.
(62) Lodge, T. P.; Hiemenz, P. C. *Polymer Chemistry*, 3rd ed.; CRC Press: Boca Raton, Florida; London; New York, 2021.
(63) Vankrevelen, D. W.; Hoftyzer, P. J. Prediction of Polymer Densities. *J. Appl. Polym. Sci.* **1969**, *13*, 871−881.
(64) Eisenberg, A. Glass Transitions in Ionic Polymers. *Macromolecules* **1971**, *4*, 125−128.
(65) Eisenberg, A.; Farb, H.; Cool, L. G. Glass transitions in ionic polymers. *J. Polym. Sci., Part A-2* **1966**, *4*, 855−868.
(66) Matsen, M. W.; Schick, M. Microphases of a Diblock Copolymer with Conformational Asymmetry. *Macromolecules* **1994**, *27*, 4014−4015.

https://doi.org/10.1021/acsapm.2c02220
ACS Appl. Polym. Mater. 2023, 5, 2223−2229